Texture direction analysis of micro-topographies using fractal geometry

Surface Topography: Metrology and Properties

OPEN ACCESS

RECEIVED
31 May 2022

REVISED
7 October 2022

ACCEPTED FOR PUBLICATION
17 October 2022

PUBLISHED
28 October 2022

PAPER

Texture direction analysis of micro-topographies using fractal geometry

Stefan Siemens , Markus Kästner and Eduard Reithmeier

Institute of Measurement and Automatic Control, Leibniz University Hannover, An der Universität 1, 30823 Garbsen, Germany

E-mail: siemens@imr.uni-hannover.de

Keywords: surface metrology, fractal geometry, texture direction, micro-topography, texture analysis, fractal dimension, power spectrum density

Abstract

In recent years fractal geometry has been repeatedly shown to help describe and characterize micro-topographies. Important properties of micro-topographies include roughness or texture direction. Consequently, in this work, fractal geometry is investigated to determine texture direction. For this purpose, synthetic data and real height maps of different micro-topographies are evaluated using the fractal power spectrum density method. The results are compared with a manual determination of the texture direction and determining the texture direction according to ISO 25 178 using the S_{td} parameter. The results show that the fractal method is more accurate than the currently standardized method. Another advantage is that secondary texture directions can be detected. Thus, the fractal method is well suited for characterizing micro-topographies and can complement existing parameters from ISO 25 178.

1. Introduction

The requirements and properties of technical components and materials, such as metallic products, are continuously increasing. Consequently, non-destructive testing methods are becoming more and more critical. They play an essential role in research and development, manufacturing, and disciplines such as tribology, precision engineering, and nanotechnology [1, 2]. Optical methods give a non-contacting and, therefore, non-damaging data acquisition option. They allow for an areal surface measurement and subsequent characterization of the surface. The micro-topography of a surface has a significant impact on its physical and chemical properties [1]. It can be specifically designed to improve existing functions or add new ones. It is possible, among other things, to change adhesion, hydrophobic, optical, tribological, biological, or fluidic properties, but also properties such as fracture toughness, fatigue strength, or electrical and thermal conductance [2, 3]. A typical example of so-called functional integration is the introduction of a microstructure into cylinder liners by plateau-honing. The cylinders have smooth plateaus intersected by valleys. The former are wear-resistant and are used for load-bearing, while the latter serves as a reservoir for lubricant and entrapment for abraded material [4]. The modified microtopography enables better wetting of the liners with oil, resulting in lower friction and oil consumption and increased service life.

Many national and international standards define parameters for characterization, among them ISO 21 920 and ISO 25 178, for 1D and 2D characterization, respectively [3, 5, 6]. A summary of typical parameters is given in [2]. Regarding the control and production of functionally integrated surfaces, important characteristics, for example, are the texture direction or lay and the surface roughness. In practice, simple statistical parameters, such as the arithmetical mean height (R_a or S_a) or maximum height (R_z or S_z), are often used to determine the roughness of a surface [7]. However, these are often insufficient. For example, different micro-topographies can result in the same roughness value [7]. Another drawback is that measures like R_a are scale-dependent. Roughness parameters obtained at different measurement scales or techniques are, therefore, not comparable [1]. Thus, further parameters are necessary for reliable characterization. Fractal methods give an additional way to quantitively characterize many micro- and macrostructures because almost all surfaces with

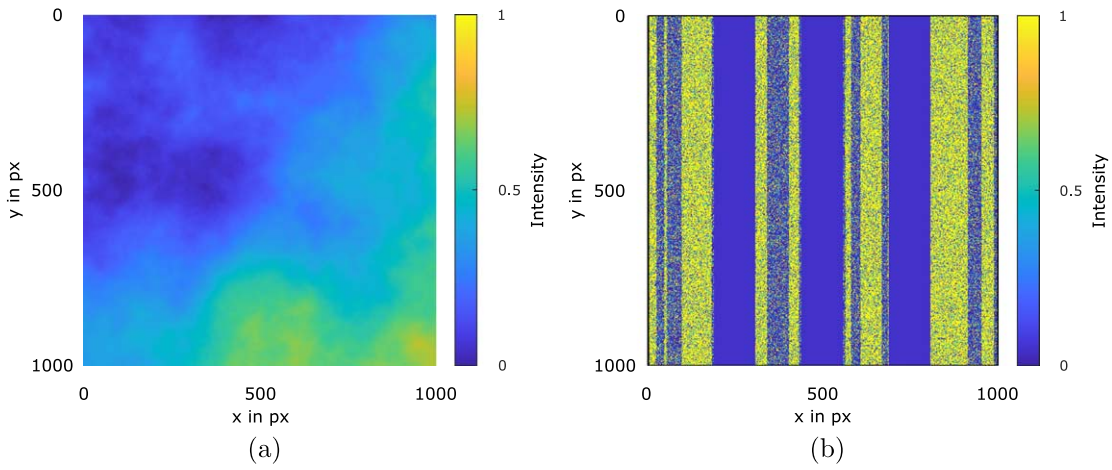

Figure 1. Example images from dataset 1 (a) and dataset 2 (b). (a) Synthetic image with a hurst exponent of 0.8147. (b) Synthetic image with a texture direction of 90°.

Table 1. Overview of the datasets used.

Dataset	Data source	Nb. of images
1: Fractal dimension estimation	Synthetically generated	200
2: Texture direction estimation	Synthetically generated	13
3: Texture direction estimation	CLSM measurements	36

engineering applications have at least some degree of fractal properties [8–11]. Moreover, fractal methods are scale-independent, allowing, for example, a direct comparison between different roughness values [1]. The literature describes fractal methods not only for evaluating roughness-like properties [7] but also for obtaining the lay or texture direction [12]. Accordingly, investigating fractal geometry for surface characterization could complement areal surface roughness parameters from ISO 25 178, and better characterize the microstructures. Consequently, this paper aims to study the fractal power spectrum density (PSD) method to determine the texture direction. For evaluation, a manual determination of the texture direction is performed. Additionally, the S_{td} parameter for the texture direction is obtained according to ISO 25 178-2:2012.

2. Materials and methods

2.1. Data

For this work, three datasets were used, see table 1. The first dataset consists of 200 synthetically generated images with a predefined Hurst exponent H and, therefore, a known fractal dimension. An example is shown in figure 1(a). These images were used to validate the fractal dimension estimation using the PSD method and were generated using Botev's algorithm with a random Hurst exponent between 0 and 1 [13]. The second dataset was used to validate the determination of the texture direction. For this purpose, 13 synthetic images with a known texture direction between 0° and 180° were generated, see figure 1(b). The third dataset consists of 13 real surfaces with six different manufacturing processes or processing methods. So-called 2.5D height maps of the microtopography were acquired using a confocal laser scanning microscope (CLSM) for each surface. Three different objectives were used, a 10x, a 20x, and a 50x magnification lens, so that a total of 36 height maps were analyzed. The material of surfaces 1–12 is a zinc alloy and an Al_2O_3 ceramics with stochastic pores for surface 13. Surfaces 1–4 are laser structured, surfaces 5–7 flat ground, surface 8 honed, surfaces 9–11 face milled, surface 12 lapped, and surface 13 thermally sprayed. According to ISO 25 178–2:2012, surfaces 1-11 have an average texture aspect ratio of $S_{tr} = 0.13$, which is strongly anisotropic, compare figure 2(a). Each of these surfaces has one or two texture directions. The ground truth for the texture directions was obtained by manually analyzing every measurement. Conversely, the average texture aspect ratio of surfaces 12-13 is $S_{tr} = 0.87$, which is strongly isotropic. Accordingly, these two surfaces have no texture direction, compare figure 2(b).

2.2. Confocal laser scanning microscopy

The model of the CLSM used for the measurements is a Keyence VK-X210. The microscope takes RGB images with a resolution of 1024 × 768 pixels. Moreover, a laser with a wavelength of 408 nm and the confocal principle is used to gather 2.5D height maps. These height maps also have a resolution of 1024 × 768 pixels. Each pixel has a corresponding

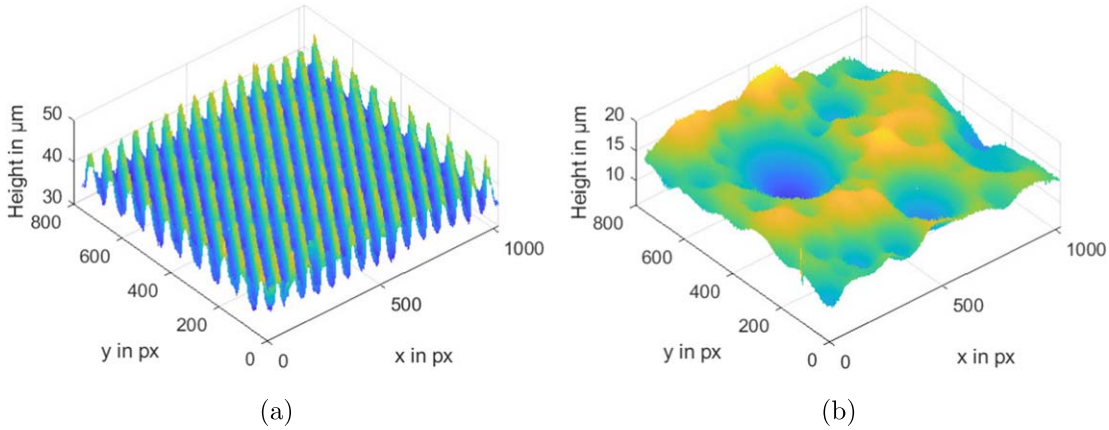

Figure 2. Example images from dataset 3. (a) Height map of a laser structured surface at 20x magnification. Primary texture direction: −50°. Secondary texture direction: +39°. (b) Height map of a lapped surface at 20x magnification. Isotrope topography without a texture direction.

Table 2. Specifications of the lenses used.

Magnification	10x	20x	50x
Numerical aperture	0.3	0.46	0.95
Measuring field	1.3 mm × 1.0 mm	0.7 mm × 0.5 mm	0.3 mm × 0.2 mm
Vertical resolution	26 nm	5 nm	2 nm
Depth of field	3.1 m	1.3 m	0.3 m
Lateral resolution	1401.869 nm/px	687.162 nm/px	277.733 nm/px

height value of the topography at that point. Analogous to a stylus instrument or a surface profiler, this data can be used to calculate parameters like the roughness of a surface. Compared to these more traditional methods, which are still the standard in many areas today, the CLSM has two main advantages [14]. First, it is non-contacting and, therefore, non-damaging. Second, it allows for areal surface measurements, and therefore a much faster and, due to the much-increased sample size, statistically more sound results. A 10x-, 20x-, and 50x magnification objective lens was used for each surface. The properties of these objectives are listed in table 2.

The filtration technique for the measurements follows ISO 25 178–3:2012. First, the Real Surface gets sampled in x and y and digitized in z to obtain the Extracted Surface. Then, measurement noise is removed by using an S-Filter, which is a Gaussian low-pass filter with a cut-off-wavelength chosen according to the lateral resolution of the respective objective. The result is the so-called Primary Surface. The form is then removed (F Operator) using a least-squares fit. This results in the SF Surface on which the parameters are then calculated.

2.3. Fractal geometry

Fractal geometry is a branch of mathematics in which, unlike in classical Euclidean geometry, objects with a non-integer dimension D are considered. When applied in image analysis, fractal geometry is often brought to the evaluation of the fractal dimension (referred to as D_F) [15]. Generally, a distinction is made between mathematical or ideal fractals and physical or real fractals. Mathematical fractals have the property of self-similarity, while physical fractals have the property of self-affinity. Self-similarity means that the fractal dimension is different from the Euclidean dimension on an infinite scale. In other words, the object shows the same or similar structures at different magnifications as in the initial state. In contrast to mathematical objects, real objects cannot be similar at infinite scales [11]. Self-affinity, therefore, is defined as a deviation from the Euclidean dimension over several, but finitely many, orders of magnitude. The fractal dimension can be considered as a relative measure of a pattern's complexity, roughness, or scale dependence [16]. A higher dimension means a higher degree of complexity and a more irregular shape or structure. The fractal dimension is relatively easy to calculate for simple, mathematical fractals. In practice, this is usually not the case. First, natural fractals are generally not deterministically self-affine. This means that an enlarged section has similarities to the whole but not precisely the same structure. Second, the scaling may vary for different magnitudes or different directions. Third, self-affinity in natural fractals does not occur over an infinite range of scales. In addition, measured data have limited resolution and are often discretized. For these reasons, the fractal dimension can usually only be estimated. There are various

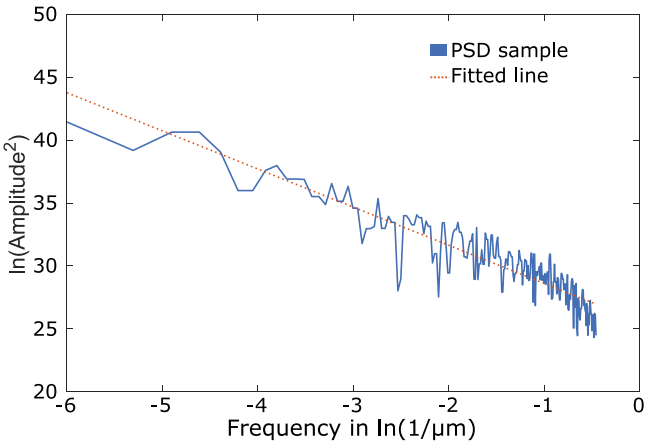

Figure 3. Determination of the fractal dimension in a PSD sample using a line fit and equation (1).

methods for this, which are not uniformly classified [16]. However, most methods follow the same principle [15]:

(i) Measurement of an object or a property at various step sizes,

(ii) Least-squares line regression through a double logarithmic display of the measured properties as a function of the step size,

(iii) Estimation of the fractal dimension using the slope of the regression line.

If the slope of the fitted line is not equal to zero, this means that the measured size changes with increasing resolution and has fractal properties.

2.4. Power spectrum density

The most commonly used method is the box-counting method [15] since it is relatively simple. However, it is unsuitable for the objective of this work, as it cannot be used to determine the directional dependence of the surface lay. Another approach to estimating the fractal dimension is using the power spectral density (PSD) plotted over the frequency spectrum. An advantage is the possibility to measure the anisotropy of a surface by determining the fractal dimension as a function of direction. Moreover, the method can be applied to both self-affine and self-similar data [17]. A disadvantage is the high computational effort and the difficult interpretation of the results [11]. The PSD is calculated by squaring the amplitude of the Fourier transformed signal. The Fourier transform calculation is done via the Fast Fourier transform (FFT). If the examined signal has fractal properties, the double logarithmic representation of the PSD has the form of a straight line. According to [17], the slope of the line m, the Euclidean dimension D, and the fractal dimension D_F are related as follows:

$$D_F = \frac{3D + 2 - |m|}{2}. \tag{1}$$

An example of the line fit is shown in figure 3.

From equation (1), it follows that errors in the line fit lead to an incorrect value for the fractal dimension. Errors can occur because outliers strongly influence the slope at the upper or lower end of the frequency spectrum. For example, measurement noise causes high amplitudes at high frequencies, which leads to a lower absolute slope. On the other hand, a low measurement resolution results in a low information content at high frequencies and, therefore, a higher absolute slope. Another problem is that low frequencies have a more significant effect on the slope due to the logarithmic scaling than high frequencies [12]. The DC component, also called the 0th frequency, measures the surface's average height, while the subsequent low frequencies measure the form and the waviness. Since the mean height is dependent on an arbitrarily chosen reference point, it is neglected for the line fit. Figure 4(a) shows a laser structured surface. In Fourier space, the texture direction would be seen by larger amplitudes perpendicular to the texture direction. As can be seen in figure 4(c), additional, spurious amplitudes occur along the image axes over a wide frequency spectrum. Large amplitudes over a broad spectrum lead to a small line slope and, according to equation (1), to a high fractal dimension D_F. These artifacts occur because the discrete Fourier transform has an implicit periodicity in the spatial and frequency domain. As shown in figure 4(b), a periodic repetition of the input signal leads to horizontal and vertical discontinuities. For this reason, the discontinuities in the time domain result in unwanted amplitudes in Fourier space and artifacts in the estimated fractal dimension, see figure 4(d). The artifacts are mitigated by dampening the strength of the periodic discontinuities. In order to do so, the input image is multiplied with a window function of the same size. The window function has a value of one at the center

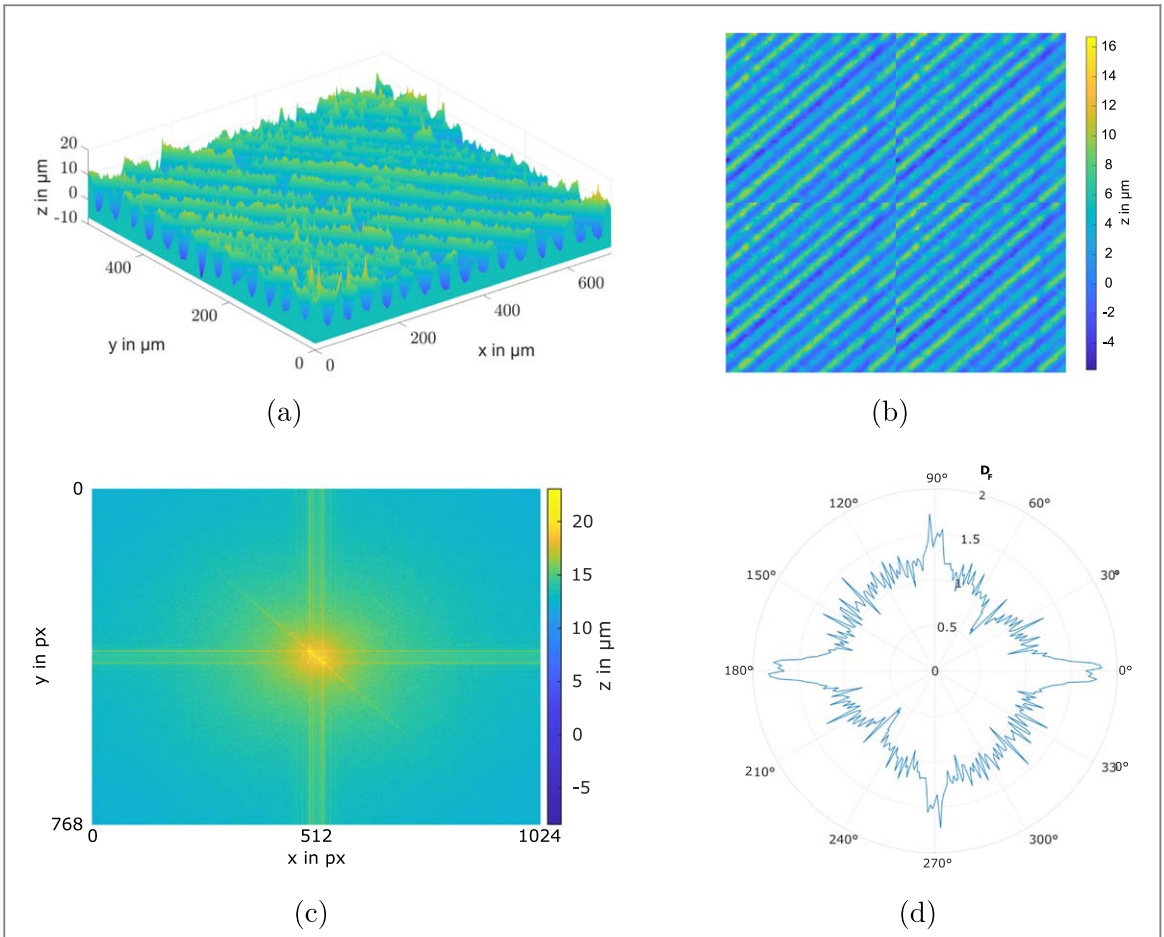

Figure 4. D_F estimation without windowing. (a) Laser structured surface (20x magnification) with a texture direction of 41deg. (b) Horizontal and vertical discontinuities in the replicated surface image. (c) Spurious amplitudes in the Fourier transformed surface. (d) Horizontal and vertical artifacts for the estimated D_F.

and decreases to zero towards the edges. In this work, the Tukey window function is used, which is shown in figure 5(a) and defined as:

$$w(x) = \begin{cases} \frac{1}{2}\left\{1 + \cos\left(\frac{2}{\pi}\left[x - \frac{r}{2}\right]\right)\right\}, & 0 \leqslant x \leqslant \frac{r}{2} \\ 1, & \frac{r}{2} \leqslant x \leqslant 1 - \frac{r}{2} \\ \frac{1}{2}\left\{1 + \cos\left(\frac{2}{\pi}\left[x - 1 + \frac{r}{2}\right]\right)\right\}, & 1 - \frac{r}{2} \leqslant x \leqslant 1. \end{cases} \quad (2)$$

Where x is a vector with equidistant entries and r is the fraction of the curve that is tapered by the cosine [18]. The advantage of this function is that the range in which the input image is dampened can be very narrow so that the signal is only perturbed in the edge area, see 5(b).

2.5. Sampling the measurement data

To investigate the anisotropy of the surfaces, a 1D sample is taken radially for each direction. The step size is 1 pixel in radial and 1° in the angular direction. The fractal dimension D_F of each 1D sample is estimated and then plotted in polar coordinates. This representation is called Hurst plot or Rose map. The direction in which the fractal dimension decreases corresponds to the texture direction of the surface [19].

2.6. Filtering the fractal dimension

The estimated D_F is subject to noise so that filtering is necessary. This is done using envelope curves, which correspond to a low-pass filter. The maximum and the minimum envelope curves are calculated throughout three neighboring points. The average value between the maximum and minimum envelope curve is taken for each sample point. Figure 6 shows an example of a surface's unfiltered and filtered fractal dimension with the maximum, minimum and the resulting medium envelope curve.

2.6.1. Determination of the texture direction

The texture direction of each image i is determined using an adaptive threshold T_i which is given by:

$$T_i = mean(D_{F,i}) - |\max(D_{F,i}) - mean(D_{F,i})|, \quad (3)$$

with $D_{F,i}$ being the fractal dimension of the i-th image. If D_F falls below T_i, the corresponding angles are marked as significant, see figure 7. The significant angles are divided into regions with a window width of

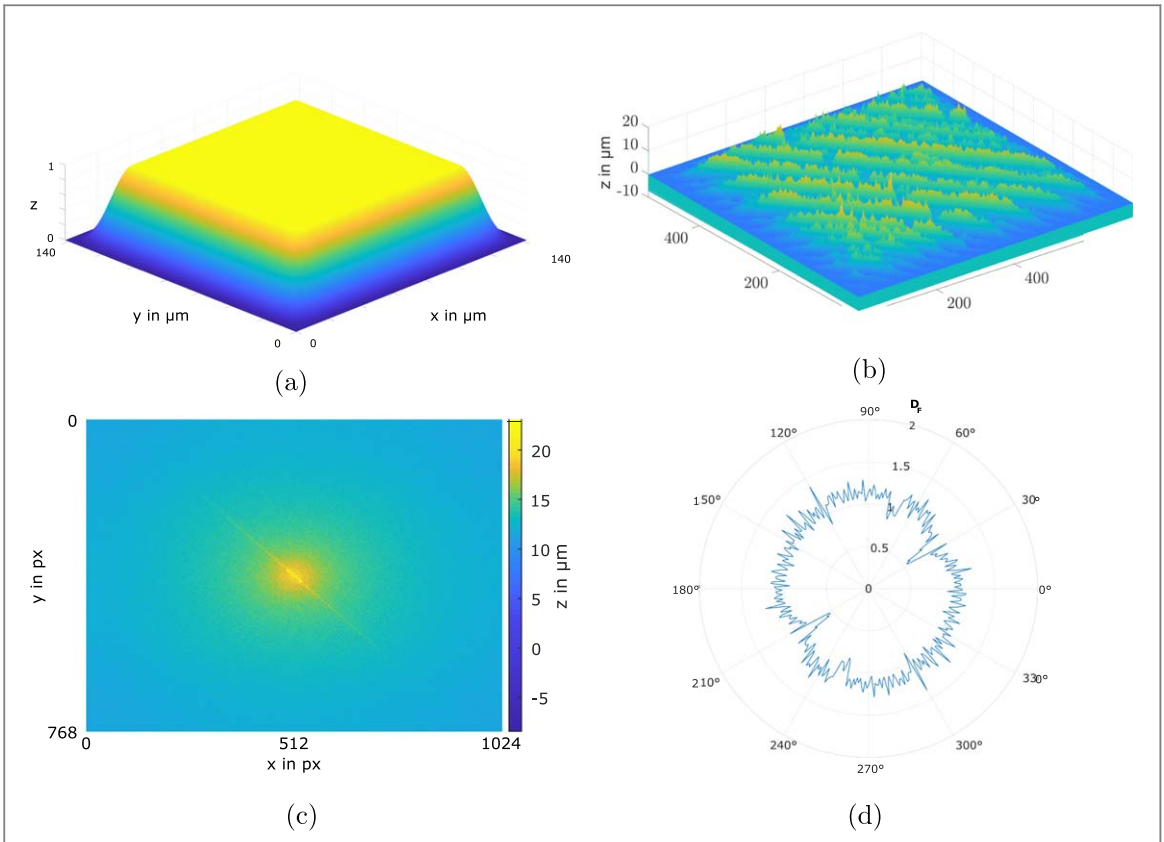

Figure 5. D_F estimation with windowing. (a) 2D Tukey window function. (b) Laser structured surface (20x magnification) with Tukey window applied. (c) Fourier space image of the surface with Tukey window applied. (d) Estimated D_F without horizontal and vertical artifacts.

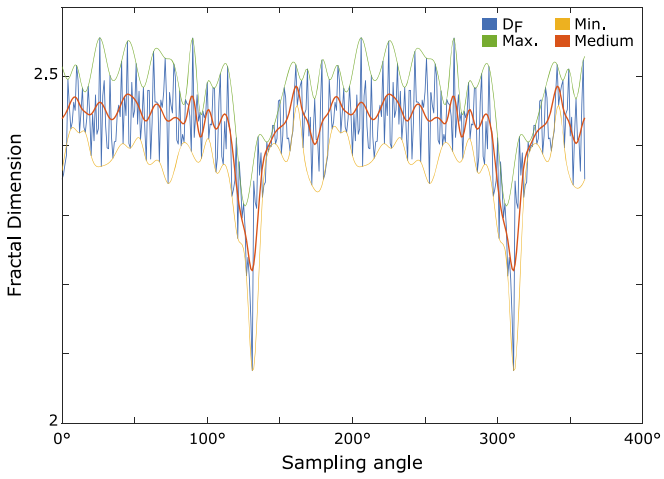

Figure 6. Example of an unfiltered and filtered fractal dimension of a surface with the maximum, minimum and the resulting medium envelope curve.

$\pm 10°$. A weighted mean value is calculated for each region to determine the exact direction.

2.7. Spatial parameters

To evaluate the performance of the PSD method, a comparison with the texture direction of the surface parameter S_{td}, defined in ISO 25 178-2:2012, is made. First, the discrete autocorrelation function of the $M - by - N$ height map H is the matrix AFC with the size $2M - 1$ by $2N - 1$. Its entries are given by:

$$AFC(k, l) = \sum_{m=0}^{M-1} \sum_{n=0}^{N-1} H(m, n)\bar{H}(m - k, n - l), \quad \text{with} \quad \begin{aligned} &-(M-1) \leqslant k \leqslant M-1, \\ &-(N-1) \leqslant l \leqslant N-1, \end{aligned} \tag{4}$$

where $\bar{H}$ is the complex conjugate of H. The function gets normalized to values between 0 and 1 and

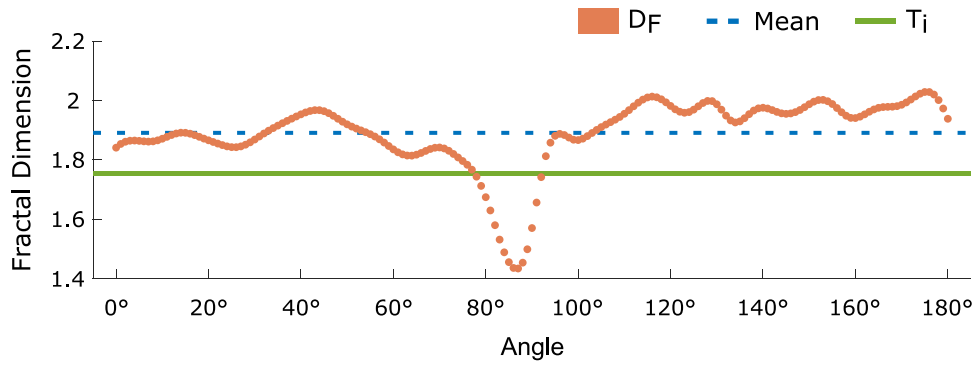

Figure 7. Example of the fractal dimension of a surface with the corresponding adaptive threshold T_i.

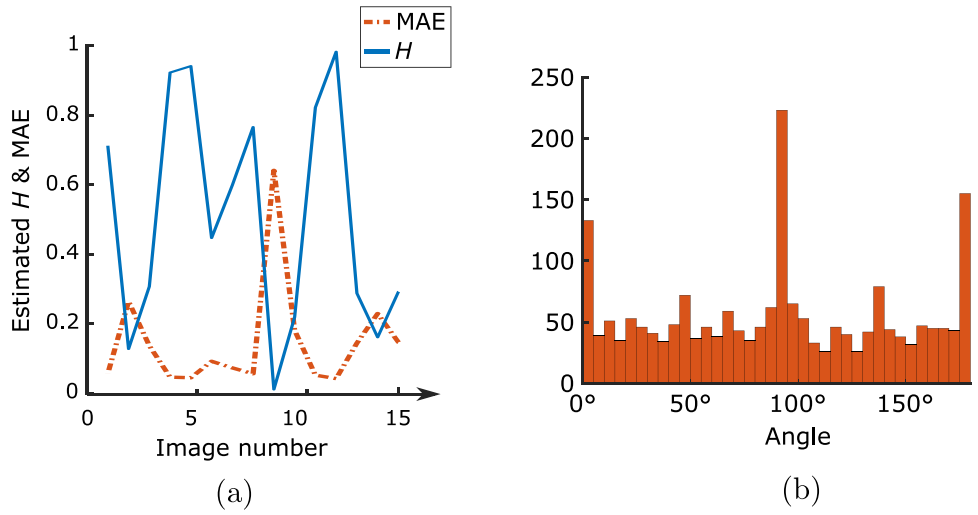

Figure 8. MAE for the Hurst estimation. (a) Estimated Hurst parameter and MAE of the estimation for the first 15 images of synthetic dataset 1. (b) Histogram of the angles with the largest MAE using the PSD method on dataset 1.

contains a central peak with the maximum amplitude. Then a threshold s with a typical value of 0.2 is applied. The shortest and the longest decay lengths $R_{\min}$ and $R_{\max}$ can be obtained from this. They are given by the shortest and the longest distance from the center of the autocorrelation function to a value below the threshold. The fastest decay auto-correlation rate S_{al} is given by $R_{\min}$ and is expressed in μm. The texture aspect ratio of the surface S_{tr} is given by $^{R_{\min}}/_{R_{\max}}$. It is a dimensionless value between 0 and 1 and is a measure for the anisotropy of a surface, with 0 being a completely isotropic and 1 being completely anisotropic. Finally, the power spectrum of the surface in each direction is calculated. The angle with the largest power spectrum corresponds to the texture direction S_{td}.

3. Results

3.1. Estimation of the fractal dimension

First, the fractal dimension prediction accuracy is evaluated using dataset 1. In accordance to [7] the Hurst exponent H is estimated with the PSD method via the relation

$$H = 3 - D_F. \tag{5}$$

The mean absolute error (MAE) between the predicted and the ground truth D_F is 0.1342, with a standard deviation of 0.1250 and a maximum error of 0.6625. Another observation is that H correlates negatively with the magnitude of the MAE. Figure 8 shows an example of the ground truth D_F and the MAE for the first 15 synthetic images. It can be seen that the error is significantly higher for low Hurst parameters and vice versa.

3.2. Estimation of the texture direction

Second, the accuracy of the direction detection with the PSD is determined using the synthetic dataset. An example of a surface with the manually determined texture direction, the corresponding Hurst plot, and the detected texture direction is shown in Figures 9 (a) and 9 (b), respectively. In comparison, Figures 10 (a) and 10 (b) show an isotrope surface and the corresponding Hurst plot. The MAE for the synthetic images is 0.76°, with a standard deviation of 0.35° and a maximum of 1.09°. Lastly, the results for estimating

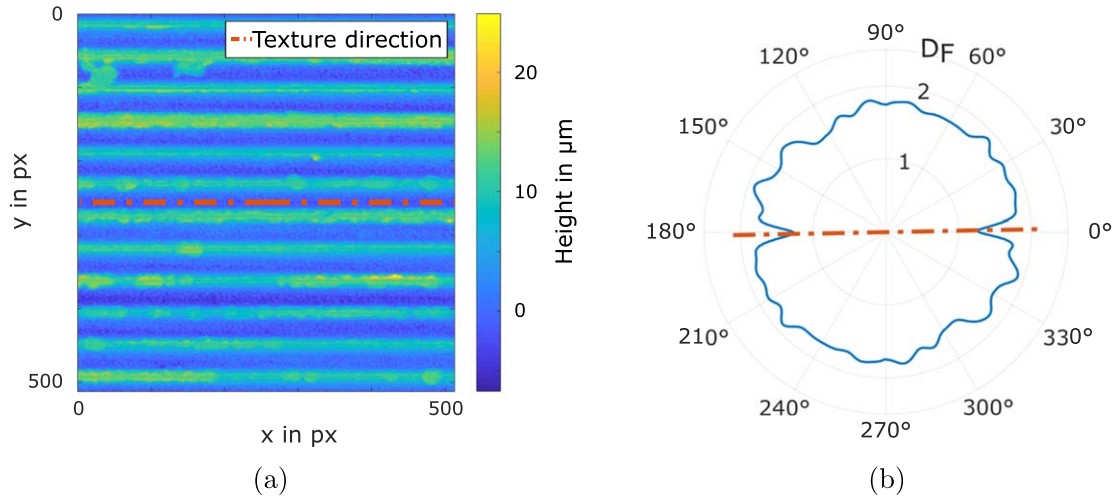

Figure 9. Laser structured surface at 20x magnification. (a) Detected texture direction of +1°. (b) Hurst plot of the filtered D_F.

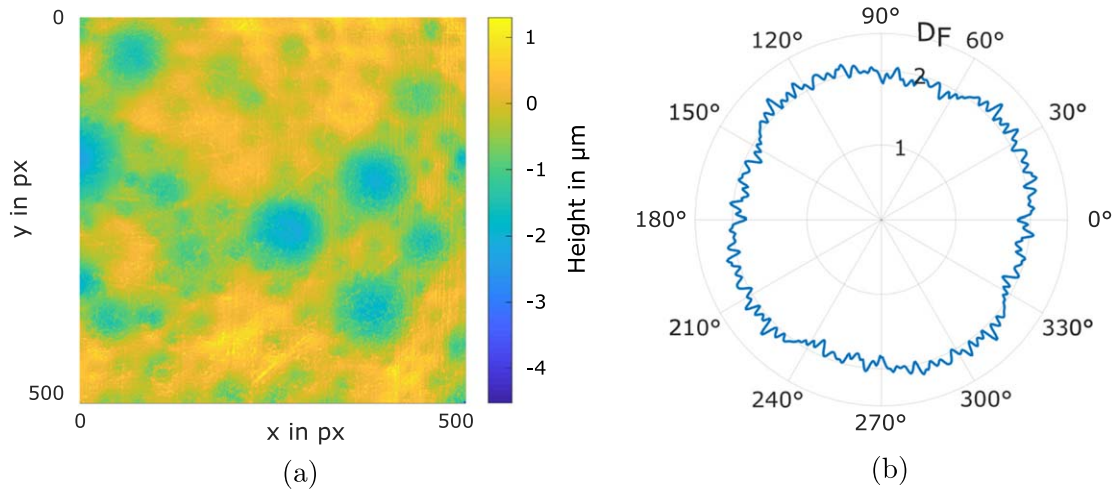

Figure 10. Lapped surface at 20x magnification. (a) Isotrope surface without a texture direction. (b) Hurst plot of the unfiltered D_F.

the texture direction using the PSD and the S_{td} method on real measurement data are shown in table 3 and figure 11.

The threshold-based PSD method is the most accurate compared to the manual determination. The MAE for the PSD method is 0.77°, the standard deviation 0.70°, and the maximum error 2°. No false positives and 2 out of 3 secondary texture directions were detected. With the S_{td} method, the MAE is 1.45°, with a standard deviation of 2.64° and a maximum of 9°. No false positives were detected with this method, while no secondary texture direction was detected.

4. Discussion

The fractal dimension of the synthetic surfaces can be well estimated by the PSD method. However, the absolute values of the estimation should be considered with caution since they can deviate significantly from the ground truth values. This result was to be expected since the values estimated by the PSD differ from the values obtained by other fractal methods. According to Russ, the PSD value is theoretically less than or equal to the true value [12]. Since only relative D_F values, or the change of D_F values, is relevant for this work, the deviations are acceptable. However, it is interesting to note that the deviations are often the largest for image samples at angles of 0°, 90°, and 180°. Since the data gets interpolated for sampling at all other angles, resulting in a loss in the high-frequency signal component, the deviations could be explained by noise or the high-frequency signal component. Consequently, filtering measurement noise according to ISO 25 178 might not be sufficient when using the PSD method, and stronger Gaussian filters or other filtering methods should be used. Another interesting observation is the relationship between the value of D_F and the magnitude of the MAE for the D_F estimation. The reason for this is unclear, as the literature on this is conflicting. For instance, Gomez-Rodriguez *et al*

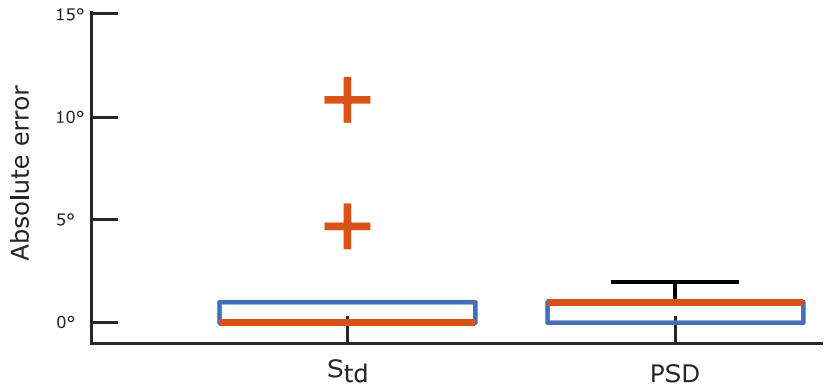

Figure 11. Absolute error of the texture direction estimation with the S_{td} (left) and the PSD method (right).

Table 3. Results of the texture direction determination using the S_{td} and the PSD method.

Surface	Manufacturing/ processing	Ground truth	S_{td}	PSD
1	Laser structuring	0°	0°	1°
2P	Laser structuring	−50°	−54°	−49°
2S	Laser structuring	39°	—	39°
3	Laser structuring	41°	41°	41°
4P	Laser structuring	89°	90°	89°
4S	Laser structuring	−2°	—	−2°
5	Flat grinding	90°	90°	91°
6	Flat grinding	90°	90°	91°
7	Flat grinding	62°	62°	62°
8P	Honing	−70°	−79°	−68°
8S	Honing	63°	—	—
9	Face milling	89°	90°	88°
10	Face milling	57°	58°	59°
11	Face milling	33°	33°	34°
12	Lapping	—	—	—
13	Thermal spraying	—	—	—
MAE			**1.45°**	**0.77°**

describe that D_F is overestimated with the PSD method for values of $D_F < 2.5$ $(0.5 > H \geqslant 1)$ and underestimated for values of $D_F > 2.5$ $(0 \leqslant H < 0.5)$, while Feder states that D_F is overestimated for values of $D_F > 2.28$ $(H < 0.72)$ and underestimated for values of $D_F < 2.28 (H > 0.72)$ [20, 21]. However, the correlation observed here could not be found in the literature, so further work is needed. Moreover, the texture direction of both synthetic and real surfaces can be determined well with the PSD method, as the MAE for both image types lies well below one degree. Although the standard deviation and the maximum error for real images are about twice as large as for synthetic images, the results agree well with each other. This validates the fractal method and the manually determined ground truth values of the real texture directions. As a caveat, the synthetic structures are relatively simplistic and are not necessarily representative of real surfaces except for the texture direction. In addition, the specific values of the fractal dimension were not investigated but only relative values to determine the texture direction. Lastly, no surfaces with multiple texture directions were generated and examined. For the real surfaces investigated, the accuracy of the threshold-based PSD method is above the accuracy of the S_{td} method of ISO 25 178, which is the state-of-the-art algorithm. This is especially true for detecting secondary texture directions. As shown in 12 (left), the primary (89°) and secondary (−2°) texture directions of surface 4are well visible to the naked eye. Nevertheless, the secondary texture direciton is not detected when using the S_{td} parameter, as is shown in 12 (right). A small peak of the secondary texture direction can be seen when magnified. However, this is not significant enough for detection with the S_{td} method. In contrast, even with the PSD method on surface 8, see figure 13 (left), no secondary texture direction is detected, although it is significantly pronounced visually and in the height data. Surface 8 is also the one with the largest error for the S_{td} parameter and, together with surface 9, for the PSD method. Compared to the other structured surfaces, surface 8 is much flatter with a significantly weaker anisotropy ($S_a = 0.36$ μm, $S_q = 0.51$ μm, $S_z = 8.13$ μm, $S_al = 8.92$ μm) than the average values ($S_a = 1.77$ μm, $S_q = 2.03$ μm, $S_z = 14.75$ μm, $S_al = 25.58\mu$ m). Figure 13 (left) shows the scaled and unfiltered Hurst lot for surface 8. However, when looking at a scaled Hurst plot both the primary and secondary texture direction can be seen by a lower fractal dimension at the angles of the texture directions. However, when looking at a scaled Hurst plot a lower fractal dimension can be seen at the angles of the primary and secondary texture direction. Due to these D_F minimums' relatively small amplitude and angular range, the secondary texture direction gets filtered out and consequently not detected by the thresholding algorithm. Therefore, improvements for both filtering and thresholding of the fractal dimension are needed.

One general criticism of the implemented method is the poor comparability with other methods. For example, the estimated fractal dimension does not correlate with roughness parameters for the investigated surfaces. Another example is that different fractal methods output different values for the fractal dimension.

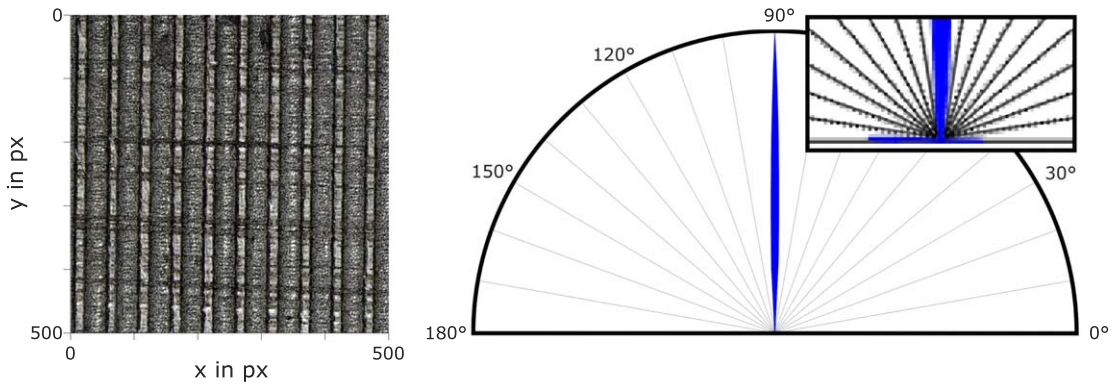

Figure 12. Left: RGB image of surface 4 (Laser structuring) at 20x magnification with primary (89°) and secondary (−2°) texture direction. Right: Corresponding polar spectrum according to ISO 25 178 with magnified view of the secondary texture direction.

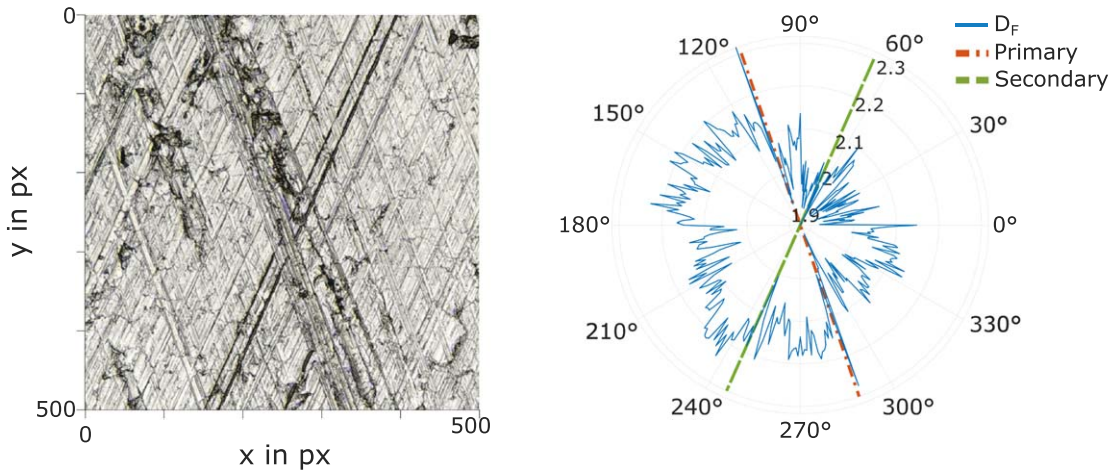

Figure 13. Left: RGB image of surface 8 (Honing) at 20x magnification with primary (−70°) and secondary (63°) texture direction. Right: Hurst plot of the unfiltered D_F with manually determined primary and secondary texture direction.

Since only relative D_F values were considered for this work, this shortcoming is justifiable. Nevertheless, for other fractal methods, without further investigations, it cannot be said how well they are suited for the determination of the anisotropy and texture direction.

5. Conclusions

This work used the fractal dimension to investigate the anisotropy of six different manufacturing processes or processing methods. Micro-topographies were measured using a CLSM with three different magnification lenses. The surfaces were radially sampled, and the fractal dimension D_F was estimated based on the power density spectrum (PSD method). Subsequently, the texture direction was determined based on D_F. The accuracy of D_F and texture direction estimation was evaluated using synthetic and real datasets. It was shown that primary as well as secondary texture directions, could be determined with high accuracy. A comparison with the texture direction calculation according to ISO 25 178 shows favorable results for the implemented method. In summary, fractal analysis is a helpful supplement to the parameters from ISO 25 178 because it allows a precise determination of the texture direction of anisotropic surfaces.

5.1. Future work

In this work, the fractal dimension was evaluated qualitatively to examine the measured data for anisotropy. The degree of anisotropy was assessed using the S_{tr} parameter. A correlation of the degree of anisotropy with the quantitative values of the fractal dimension would be interesting. Furthermore, further development of the thresholding and filtering methods could improve texture direction detection, especially secondary texture directions.

Data availability statement

The data that support the findings of this study are available upon reasonable request from the authors.

ORCID iDs

Stefan Siemens https://orcid.org/0000-0002-6203-8480

References

[1] Gong Y, Xu J and Buchanan R C 2018 Surface roughness: A review of its measurement at micro-/nano-scale *Physical Sciences Reviews* **3** 20170057

[2] Magsipoc E, Zhao Q and Grasselli G 2020 2D and 3D roughness characterization *Rock Mech. Rock Eng.* **53** 1495–519

[3] Jacobs T D B, Junge T and Pastewka L 2017 Quantitative characterization of surface topography using spectral analysis *Surface Topography: Metrology and Properties* **5** 013001

[4] Grabon W and Pawlus P 2014 Description of two-process surface topography *Surface Topography: Metrology and Properties* **2** 025007

[5] 2021 *ISO 21 920-2:2021 Geometrical product specifications (GPS)Surface texture: ProfilePart 2: Terms, definitions and surface texture parameters. English. Geneva, Switzerland: International Organization for Standardization* pp 1–78 (https://www.iso.org/standard/72226.html)

[6] 2021 *ISO 25 178-2:2021 Geometrical product specifications (GPS)Surface texture: ArealPart 2: Terms, definitions and surface texture parameters. English. Geneva, Switzerland: International Organization for Standardization*,pp 1– 64 (https://www.iso.org/standard/74591.html)

[7] Gong Y *et al* 2016 Surface roughness measurements using power spectrum density analysis with enhanced spatial correlation length *J. Phys. Chem.* C **120** 22358–64

[8] Ramos G Q, Matos R S and Duarte Da Fonseca Filho H 2020 Advanced microtexture study of anacardium occidentale l. leaf surface from the amazon by fractal theory *Microsc. Microanal.* **26** 989–96

[9] Ţălu Ş *et al* 2014 Characterization of surface roughness of Pt Schottky contacts on quaternary n-Al0.08In0.08Ga0.84N thin film assessed by atomic force microscopy and fractal analysis *J. Mater. Sci., Mater. Electron.* **25** 466–77

[10] Kanygina O N *et al* 2016 Fractal approach to the analysis of ceramic surfaces *Glass and Ceramics (English translation of Steklo i Keramika)* **72** 444–8

[11] Mainsah E, Greenwood J A and Chetwynd D G 2001 *Metrology and Properties of Engineering Surfaces* ed E Mainsah, J A Greenwood and D G Chetwynd 1 (New York: Springer Science) (https://doi.org/10.1007/978-1-4757-3369-3)

[12] Russ J C 1994 *Fractal Surfaces* 1 (New York: Springer Science) (https://doi.org/10.1007/978-1-4899-2578-7)

[13] Biagini F, Hu Y, Øksendal B and Zhang T 2008 *Stochastic Calculus for Fractional Brownian Motion and Applications* (*Probability and Its Applications*) (London: Springer London) (https://doi.org/10.1007/978-1-84628-797-8)

[14] Mínguez Martínez A and de Vicente y Oliva J 2019 Industrial calibration procedure for confocal microscopes *Materials* **12** 4137

[15] Lopes R and Betrouni N 2009 Fractal and multifractal analysis: A review *Med. Image Anal.* **13** 634–49

[16] Ţălu Ş 2012 Mathematical methods used in monofractal and multifractal analysis for the processing of biological and medical data and images *International Journal of the Bioflux Society (ABAH Bioflux)* **4** 1–4 (http://www.abah.bioflux.com.ro/docs/ABAH_4.1.1.pdf)

[17] Turner M J, Blackledge J M and Andrews P R 1998 *Fractal Geometry in Digital Imaging* (San Diego, CA: Academic)

[18] Bloomfield P 2004 *Fourier Analysis of Time Series: An Introduction* (*Wiley Series in Probability and Statistics*) 2 (New York: Wiley-Interscience) 288

[19] Hall P and Davies S 1995 On direction-invariance of fractal dimension on a surface *Applied Physics A Materials Science & Processing* **60** 271–4

[20] Gómez-Rodríguez J M *et al* 1992 Fractal Surfaces of Gold and Platinum Electrodeposits: Dimensionality Determination by Scanning Tunneling Microscopy *The Journal of Physical Chemistry* **96** 347–50

[21] Feder J 1988 *Fractals* (*Physics of Solids and Liquids*) 1 (New York: Springer Science) (https://doi.org/10.1007/978-1-4899-2124-6)